Title

Combinatorial interactions of genetic variants in human cardiomyopathy

Journal

Nature Biomedical Engineering, 3(2)

ISSN

2157-846X

Authors

Deacon, Dekker C

Happe, Cassandra L

Chen, Chao

et al.

Publication Date

2019-02-01

DOI

10.1038/s41551-019-0348-9

Peer reviewed

nature biomedical engineering

ARTICLES

https://doi.org/10.1038/s41551-019-0348-9

Combinatorial interactions of genetic variants in human cardiomyopathy

Dekker C. Deacon[1,8], Cassandra L. Happe[2,8], Chao Chen[1,8], Neil Tedeschi[1], Ana Maria Manso[1,3], Ting Li[1], Nancy D. Dalton[1], Qian Peng[4,5], Elie N. Farah[1], Yusu Gu[1], Kevin P. Tenerelli[2], Vivien D. Tran[2], Ju Chen[1], Kirk L. Peterson[1], Nicholas J. Schork[5], Eric D. Adler[1], Adam J. Engler[2,6*], Robert S. Ross[1,3*] and Neil C. Chi[1,7*]

Dilated cardiomyopathy (DCM) is a leading cause of morbidity and mortality worldwide; yet how genetic variation and environmental factors impact DCM heritability remains unclear. Here, we report that compound genetic interactions between DNA sequence variants contribute to the complex heritability of DCM. By using genetic data from a large family with a history of DCM, we discovered that heterozygous sequence variants in the *TROPOMYOSIN 1* (*TPM1*) and *VINCULIN* (*VCL*) genes cosegregate in individuals affected by DCM. In vitro studies of patient-derived and isogenic human-pluripotent-stem-cell-derived cardiomyocytes that were genome-edited via CRISPR to create an allelic series of *TPM1* and *VCL* variants revealed that cardiomyocytes with both *TPM1* and *VCL* variants display reduced contractility and sarcomeres that are less organized. Analyses of mice genetically engineered to harbour these human *TPM1* and *VCL* variants show that stress on the heart may also influence the variable penetrance and expressivity of DCM-associated genetic variants in vivo. We conclude that compound genetic variants can interact combinatorially to induce DCM, particularly when influenced by other disease-provoking stressors.

Dilated cardiomyopathy (DCM), due to multifactorial aetiologies including environmental or genetic causes, affects as many as 1 in 250 individuals and is a leading cause of morbidity and mortality worldwide[1,2]. Although more than 1,000 disease-causing variants in over 40 cardiomyopathy-associated genes have been identified, they only account for ~30–60% of the basis for familial cardiomyopathies and frequently have variable penetrance and expressivity[1,3–5]. As a result, recent human genetic studies have suggested that a substantial fraction of unaccounted cardiomyopathy heritability may be due to a combination of multigenic causes and gene–environment interactions[1,6–10]; yet, the functional evidence for these possible aetiologies remains incompletely understood.

Results

Human genetic studies reveal complex inheritance of DCM. To explore how cardiomyopathy-associated genetic variants may act combinatorially to promote DCM, we identified a family with multiple generations of DCM harbouring novel variants in the sarcomeric gene *TROPOMYOSIN 1* (*TPM1*) and the costameric gene *VINCULIN* (*VCL*; Fig. 1). The proband initially presented with severe heart failure and required heart transplantation at age 14 (Fig. 1, arrowhead and Table 1, Patient A). Further examination of an extended pedigree revealed five additional family members who developed variable presentations of cardiomyopathy across a wide age range (Fig. 1 and Table 1), including the proband's father, who was diagnosed with DCM at age 35 and his sister, who later died from sudden cardiac death at age 15 and displayed early signs of cardiomyopathy on autopsy (Supplementary Fig. 1 and Table 1). Genetic testing of the proband, his sister and his parents identified the *TPM1* and *VCL* heterozygous variants *TPM1* c.97G>A (p.Glu33Lys, p.E33K) and *VCL* c.659dupA (p.Asn220fs, p.N220fs) hereafter referred to as *TEK* (TPM1 p.E33K) and *VFS* (*VCL* frame shift), respectively. Although other *TPM1* and *VCL* variants have been associated with DCM, hypertrophic cardiomyopathy and left-ventricular non-compaction cardiomyopathy[3,11], these novel *TEK* and *VFS* variants have not been previously analyzed (Table 2). Thus, we confirmed that the *VFS* variant insertion results in a translational frame shift of VCL and a predicted premature stop at codon 240, which leads to nonsense-mediated messenger RNA decay of the *VCL* transcript and reduced VCL protein expression without evidence of truncated VCL peptide expression in skin fibroblasts harbouring both heterozygous *VFS* and *TEK* variants (Supplementary Fig. 2a–e). On the other hand, the *TEK* variant results in a change from a negatively charged glutamic acid residue to a positively charged lysine residue at codon 33 of TPM1 (Supplementary Fig. 2f). Notably, this TPM1 E33 residue is highly conserved and located in the first of three alpha helical turns that also contain the highly conserved amino acids E40 and E54, which exhibit similar variant changes (E40K and E54K) that have been associated with DCM (Supplementary Fig. 2h–j)[12,13].

Further analyses of these *TEK* and *VFS* variants in 27 additional family members revealed that affected individuals carry both of these variants (*TV-Dhet*: *TEK*-, *VFS*-double heterozygote) but never either variant alone (Fig. 1 and Table 2). However, because *TV-Dhet* variants were detected in four other family members without obvious clinical evidence of cardiomyopathy, we evaluated whether these variants, in combination or alone, were statistically correlated with disease. Evaluations using both mixed linear model association

[1]Division of Cardiology, Department of Medicine, University of California, San Diego, La Jolla, CA, USA. [2]Department of Bioengineering, University of California, San Diego, La Jolla, CA, USA. [3]Veterans Administration Healthcare San Diego, San Diego, CA, USA. [4]Department of Neuroscience, The Scripps Research Institute, La Jolla, CA, USA. [5]Department of Human Biology, J. Craig Venter Institute, La Jolla, CA, USA. [6]Sanford Consortium for Regenerative Medicine, La Jolla, CA, USA. [7]Institute of Genomic Medicine, University of California, San Diego, La Jolla, CA, USA. [8]These authors contributed equally: Dekker C. Deacon, Cassandra L. Happe, Chao Chen. *e-mail: aengler@ucsd.edu; rross@ucsd.edu; nchi@ucsd.edu

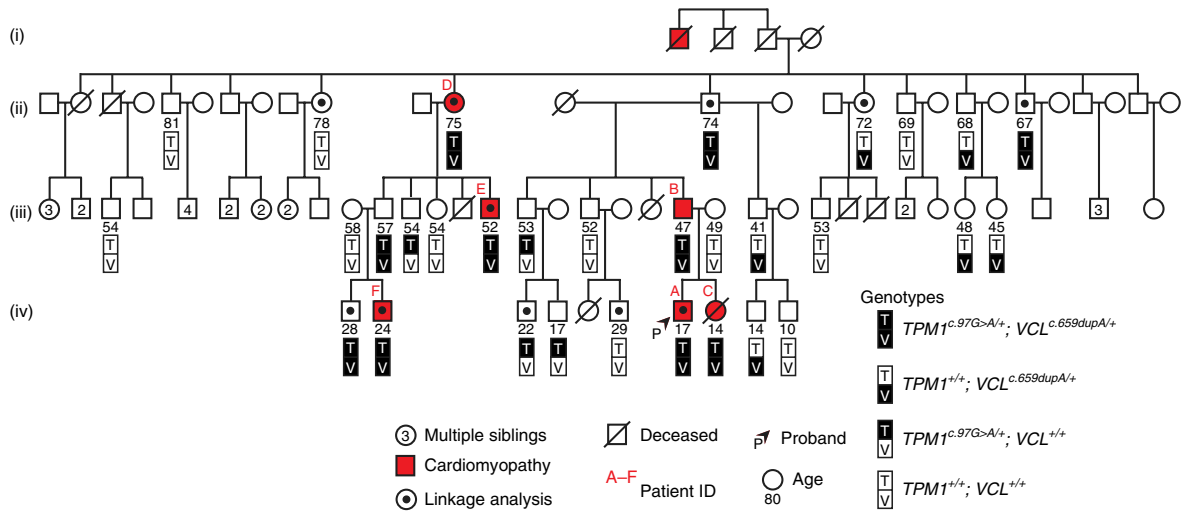

Fig. 1 | Novel *TPM1* and *VCL* variants together cosegregate with family members exhibiting cardiomyopathy. The pedigree of a large family exhibiting DCM reveals that *TPM1* and *VCL* variants cosegregate with disease (red). Age at the time of genetic testing is shown, for four generations (labelled (i)–(iv)).

Table 1 | The onset and severity of cardiomyopathy are variable in *TV-Dhet* patients

Patient	Sex	Diagnosis	Age of onset (yr)[a]	Left ventricular ejection fraction (%)	Left ventricular D/S diameter (cm)	Therapy/intervention
A	M	DCM	14	25	8.6/7.6	Left ventricular assist device/ orthotopic heart transplant
B	M	DCM	35	40	6.9/5.4	Automatic implantable cardioverter-defibrillator
C	F	Sudden cardiac death, mild hypertrophy consistent with early DCM	15	61	4.46/3.0	N/A
D	F	DCM	60	45	5.9/3.5	Medical therapy
E	M	DCM	50	46	6.1/4.5	Medical therapy
F	M	DCM	0.5	29	6.4/5.5	Mitral valve annuloplasty

The clinical characteristics of affected individuals marked in Fig. 1 with a red patient identifier (A–F) are described. The mean age of onset ± s.d. was calculated. Cardiac function is represented as left ventricular ejection fraction. The left ventricular diameter was measured during the diastole (D) and systole (S) phases. M, male; F, female; N/A, not applicable. [a]Mean = 29.1 ± 23.1.

and Fisher's exact analyses between genotype and disease showed that the *TV-Dhet* genotype associates significantly with cardiomyopathy but the $TPM1^{TEK/+}$; $VCL^{+/+}$ and $TPM1^{+/+}$; $VCL^{VFS/+}$ genotypes do not because there were no individuals with these single variant genotypes that exhibited cardiomyopathy in our pedigree (Table 2, Genotype summary). Examination of the *TEK* and *VFS* variants independent of genotype revealed that each variant segregates with disease by association beta and Fisher's exact test values, but to a lesser degree than the *TV-Dhet* genotype variant combination because a substantial number of unaffected individuals harboured either variant alone (Table 2, Variant summary). Moreover, assuming a population prevalence of DCM at 1:250, the odds ratio for the *TV-Dhet* genotype was 375 (95% confidence interval (CI): 97.8–1,436.0), whereas the odds ratios for the $TPM1^{TEK/+}$; $VCL^{+/+}$ and $TPM1^{+/+}$; $VCL^{VFS/+}$ genotypes could not be determined due to the absence of affected individuals with these genotypes (Table 2). However, when each variant was analysed independently of genotype (Table 2), the odds ratios for the *TEK* and *VFS* variants were 187.5 (95% CI: 59.36–592.2) and 150 (95% CI: 49.5–454.0), respectively. Finally, to determine whether the heritability of DCM might extend beyond the *TPM1* and *VCL* genes, we used single-nucleotide-variant microarrays to generate a high-resolution linkage map between common variants and disease using the individuals marked in Fig. 1. This analysis revealed that no single chromosomal region is shared exclusively by the affected family members and that no large structural variation exists in the genomes of selected members of this cohort (Supplementary Figs. 3 and 4). These statistical analyses therefore provide strong evidence that the *TEK* and *VFS* variants together are more closely linked to DCM than either variant alone in our pedigree, thus supporting the combinatorial role of these variants in DCM.

Human pluripotent stem cell (hPSC) cardiomyocyte modelling of DCM. To investigate the impact of these *TPM1* and *VCL* variants on human DCM pathogenesis, we generated cardiomyocytes from patient-derived human induced pluripotent stem cells (hiPSC) and clustered regularly interspaced short palindromic repeats (CRISPR–CRISPR associated protein 9 (Cas9) genome-edited isogenic H9 human embryonic stem cells (hESC). Skin fibroblasts from the DCM proband and his unaffected mother (control, CTRL), who does not carry either *TEK* or *VFS* variants, were successfully reprogrammed into hiPSCs that express pluripotency markers (Supplementary Fig. 5c)[14]. Using CRISPR–Cas9 technology, heterozygous *TEK* and *VCL c.74del7* (*VFS1*) variants

Table 2 | Cardiomyopathy associates most significantly with the *TV-Dhet* genotype in this family

Genotype summary	Abbreviation	Cardiomyopathy	Unaffected	Odds ratio (95% CI)	Association beta ± s.e.	Corrected *P* value	Fisher's exact *P* value	Frequency
TPM1$^{c.97G>A/+}$; *VCL*$^{c.659dupA/+}$	*TV-Dhet*	6	4	375 (97.8-1,436.0)	0.5711 ± 0.1084	2.40×10^{-5}	7.7268×10^{-5}	N/A
TPM1$^{c.97G>A/+}$; *VCL*$^{+/+}$	*TEK*	0	4	N/A	N/A	N/A	N/A	N/A
TPM1$^{+/+}$; *VCL*$^{c.659dupA/+}$	*VFS*	0	6	N/A	N/A	N/A	N/A	N/A
TPM1$^{+/+}$; *VCL*$^{+/+}$	*WT*	0	11	N/A	N/A	N/A	N/A	N/A
Variant summary								
TPM1$^{c.97G>A}$	*TEK*	6	8	187.5 (59.36-592.2)	0.4340 ± 0.1199	2.22×10^{-3}	2.65×10^{-3}	Not observed[a]
VCL$^{c.659dupA}$	*VFS*	6	10	150 (49.5-454.0)	0.4036 ± 0.1156	3.13×10^{-3}	8.27×10^{-3}	1/120,760 alleles

Genotype analysis shows that all individuals diagnosed with cardiomyopathy harbour the *TV-Dhet* genotype, which is significantly associated with disease by both mixed linear model association analysis ($P=2.40\times10^{-5}$) and two-sided Fisher's exact test ($P=7.7268\times10^{-5}$). In addition, the odds ratio for the *TV-Dhet* genotype is 375 (95% CI: 97.8–1,436). Because neither the *TPM1*$^{c.97G>A/+}$; *VCL*$^{+/+}$ nor the *TPM1*$^{+/+}$; *VCL*$^{c.659dupA/+}$ genotype was observed in affected individuals, the association beta values, Fisher's exact test values and odds ratio could not be statistically determined (N/A, not applicable). Analysis of *TPM1* c.97G>A and *VCL* c.659dupA variants independent of genotype revealed that each variant is not only rare (frequency) but also segregates with disease by association beta and Fisher's exact tests. However, these individual variants associate with disease to a lesser degree than the *TV-Dhet* genotype combination because each variant is observed not only together in affected individuals but also alone in unaffected individuals. [a]*TPM1* c.97G>A was not observed in exome data with coverage of flanking variants between 49,966–69,152 alleles.

were individually introduced into H9 hESCs and confirmed for targeting specificity as previously reported (Supplementary Fig. 5a,b,d and Supplementary Table 1)[15]. Similar to the *VFS* variant, the *VCL c.74del7* allele also results in an early *VCL* frame shift and subsequent decreased VCL protein levels due to nonsense-mediated mRNA decay (Supplementary Fig. 6). Employing a highly efficient cardiac differentiation protocol[16,17], these hiPSC and genome-edited hESC lines were successfully differentiated into cardiomyocytes of comparable maturity to investigate whether these variants influence cardiomyocyte function (Supplementary Fig. 5e–h). Traction force microscopy revealed a significant decrease in *VCL*$^{VFS1/+}$ hESC- and *TV-Dhet* hiPSC-cardiomyocyte contractility, as well as a trend towards reduced contractility in *TPM1*$^{TEK/+}$ hESC cardiomyocytes when compared with control hiPSC (CTRL) or hESC (*WT*) cardiomyocytes; however, the greatest reduction was observed in *TV-Dhet* hiPSC cardiomyocytes (Fig. 2a–f). Furthermore, α-actinin immunostaining of these hPSC cardiomyocytes revealed that sarcomeric organization is reduced in *TV-Dhet* and *VCL*$^{VFS1/+}$ cardiomyocytes but not in *TPM1*$^{TEK/+}$ or control cardiomyocytes (Fig. 2g–j). Overall, these functional data support that *TPM1* and *VCL* variants act synergistically to impact cardiomyocyte contractility and sarcomeric organization and suggest that together these variants may perturb sarcomeric–costameric interactions.

Gene expression analysis in DCM cardiomyocytes. To further explore the mechanistic underpinnings of these morphological and functional defects in *TV-Dhet* hiPSC cardiomyocytes, RNA-sequencing (RNA-seq) analyses were performed on biological replicates of proband (*TV-Dhet*) and unaffected (familial control) hiPSC cardiomyocytes. These RNA-seq replicates not only clustered by genotype when comparing differentially expressed genes (Fig. 3a) but also revealed 434 genes that are upregulated ($n=210$) or downregulated ($n=224$) in *TV-Dhet* hiPSC cardiomyocytes (Supplementary Table 2), including *VCL* (Fig. 3e), which was also reduced in the fibroblasts of the proband (Supplementary Fig. 2b). Supporting that the *VFS* variant is sufficiently expressed to result in this decreased *VCL* mRNA level in *TV-Dhet* hiPSC cardiomyocytes, percentage spliced-in analysis revealed complete inclusion of the exon (exon 6) containing the *VFS* variant in *TV-Dhet* hiPSC cardiomyocytes (Supplementary Table 3). Furthermore, analysis of the upregulated genes in *TV-Dhet* hiPSC cardiomyocytes showed significant enrichment for gene ontology terms related to both costameric (VCL-related) function—including extracellular matrix (ECM) organization, regulation of cell–substrate adhesion, cell–cell adhesion via plasma-membrane adhesion molecules and non-integrin membrane–ECM interaction—as well as sarcomeric (TPM1-related) function, such as muscle contraction, regulation of blood pressure and actin filament based process (Fig. 3b). In addition, biological pathways that are activated during the pathogenesis of heart failure, including oxidative stress (gene ontology term: oxidation–reduction process, reactive oxygen species metabolic process)[18], cardiac fibrosis and remodelling (gene ontology term: transforming growth factor-β receptor signalling pathway)[19] and glycolysis (gene ontology term: response to nutrient levels and cellular carbohydrate catabolic processes), are also increased in *TV-Dhet* hiPSC cardiomyocytes[20]. Conversely, genes related to signalling pathways downstream of the G-protein coupled receptor β-adrenergic receptor (gene ontology term: cAMP signalling, adenylate cyclase-modulating G-protein coupled receptor signalling pathway) are downregulated, as is typically observed during human heart failure[21]. Moreover, genes related to biological pathways that regulate blood-vessel development and response to hypoxia were also notably reduced, which is consistent with similar findings that were recently reported in *TITIN* mutation hiPSC cardiomyocytes from DCM patients (Fig. 3b)[22].

To illuminate cardiac-protein interaction complexes that may become activated due to the *TV-Dhet* variants, we performed STRING database interaction mapping[23] of differentially regulated genes associated with *VCL* (ECM organization genes) and *TPM1* (muscle contraction genes; Fig. 3c,d). Upregulation of sarcomere (Fig. 3f, red oval—MYH7, TNNC1 and MYL2) and costamere–ECM bridging (Fig. 3f, blue oval—LAMB2, LAMB3, ITGA8 and NPNT) protein network complexes was observed when plotting the proteins of these altered genes with TPM1, VCL and limited first-degree interacting proteins. Together, these data suggest that costameric and sarcomeric protein networks may be

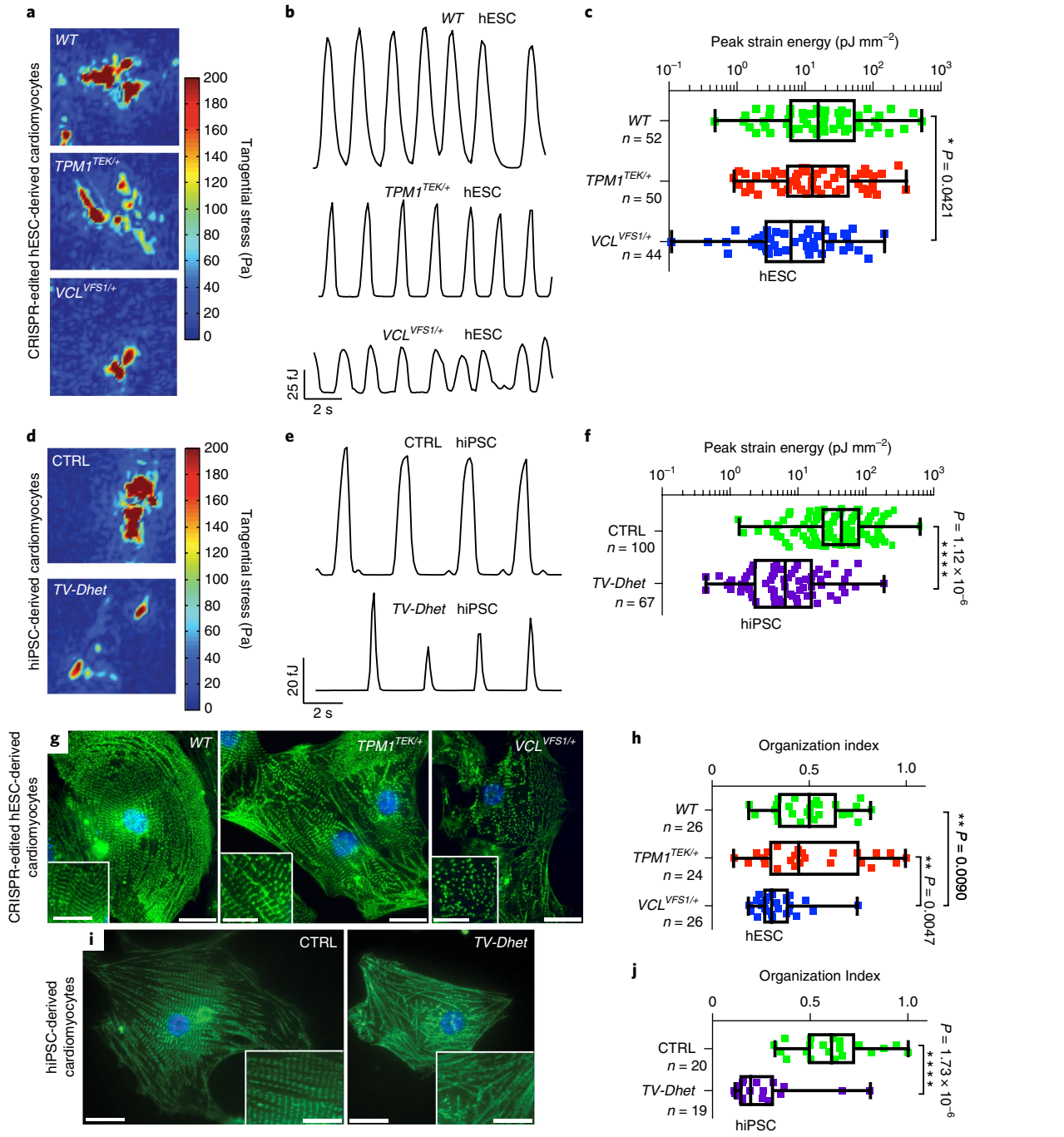

Fig. 2 | hPSC-derived cardiomyocytes harbouring *TEK*; *VCL* genetic variants exhibit functional and sarcomeric organization defects. a–**f**, Single-cardiomyocyte traction force microscopy studies show that *TV-Dhet* and $VCL^{VFS1/+}$ hPSC-derived cardiomyocytes exhibit reduced contractility as detected by tangential stress heat maps (**a**,**d**), strain energy time courses (**b**,**e**) and peak strain energy analyses (**c**,**f**). **g**–**j**, Alpha-actinin immunostaining (green; **g**,**i**) and quantitation of the sarcomeric organization (**h**,**j**) reveal that sarcomeres of *TV-Dhet* and $VCL^{VFS1/+}$ hPSC-derived cardiomyocytes are more disorganized than that of *WT* and CTRL cardiomyocytes. Control hESC-derived (*WT*) and CRISPR-edited-hESC-derived cardiomyocytes are represented in **a**–**c**,**g**,**h**. Control hiPSC-derived (CTRL) and cardiomyopathy-affected patient (*TV-Dhet*) hiPSC-derived cardiomyocytes are represented in **d**–**f**,**i**,**j**. Data are presented as interquartile range (box) around the mean (horizontal line), whiskers represent the minimum and maximum of the dataset, with the individual data points superimposed. $^{*}P < 0.05$, $^{**}P < 0.01$, $^{***}P < 0.001$ and $^{****}P < 0.0001$; two-sided Student's *t*-test (**f**,**j**) or one-sided ANOVA with Tukey multiple correction test alpha (**c**,**h**). **g**,**i**, The representative images shown were obtained from experiments independently repeated three times with similar results; Hoechst nuclear labelling is shown in blue. Scale bars, 20 µm. Inset scale bars, 10 µm. *n*, number of biologically independent cardiomyocytes of each genotype used for each study.

coordinately regulated in *TV-Dhet* cardiomyocytes as compensatory mechanisms in response to the combinatorial effects of TPM1 and VCL dysfunction.

Mouse complex genetic model phenocopies human DCM family. Finally, on the basis of the variable penetrance and expressivity of DCM in family members harbouring *TV-Dhet* variants

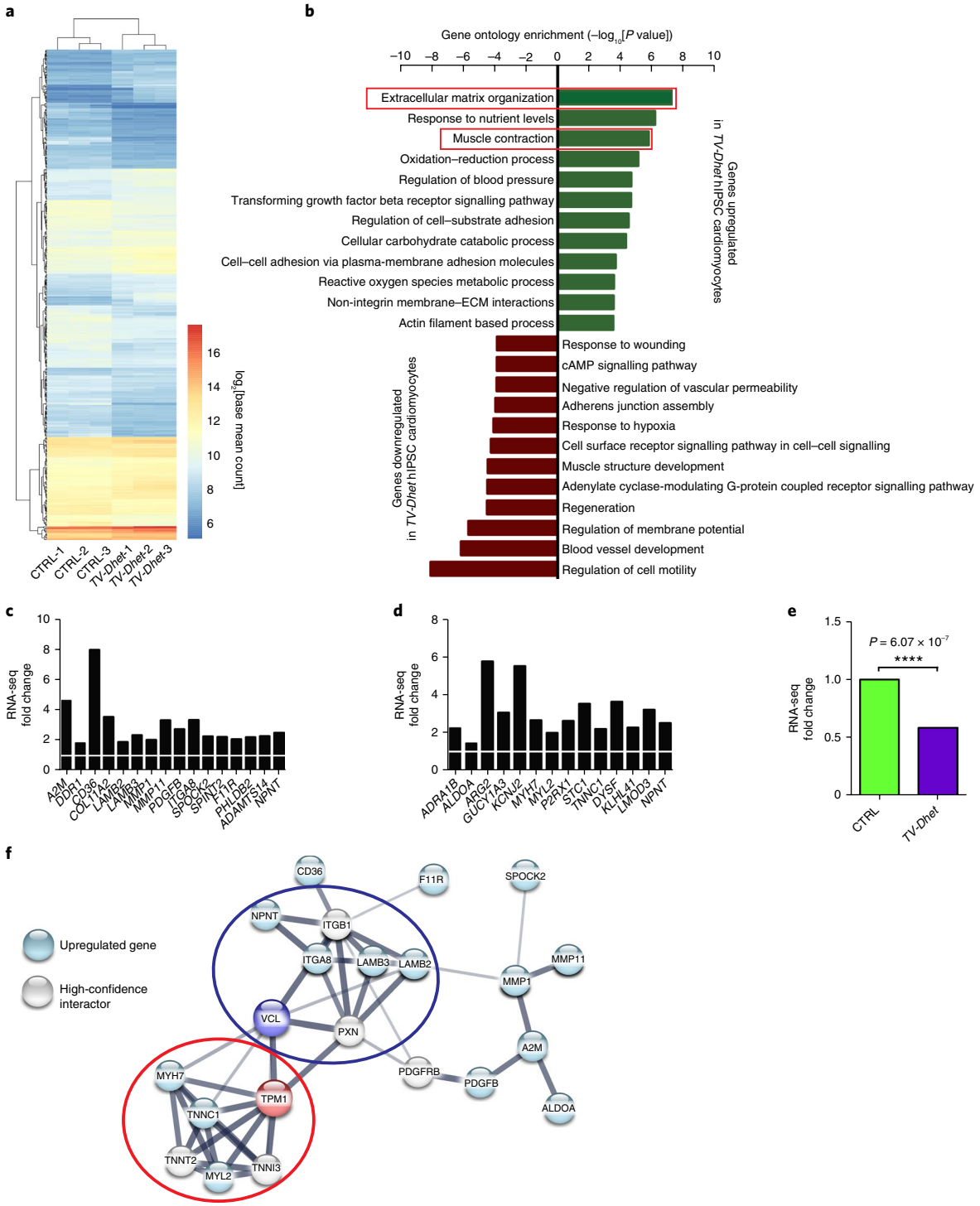

Fig. 3 | ECM and muscle contraction genes are coordinately upregulated in *TV-Dhet* hiPSC cardiomyocytes. a, Hierarchical clustering of differentially expressed genes between control (CTRL) and cardiomyopathy-affected patient (*TV-Dhet*) hiPSC-derived cardiomyocytes ($n = 3$ biological replicates per genotype) reveals clusters of genes that are coordinately regulated in *TV-Dhet* cardiomyocytes. Gene expression data from these replicates were combined by genotype in **b**–**f** to further compare relative gene expression changes. **b**, ECM organization and muscle contraction gene ontology terms are significantly enriched among genes upregulated in *TV-Dhet* cardiomyocytes whereas various gene ontology terms affecting biological processes that are regulated in heart failure are enriched among downregulated genes when using one-sided accumulative hypergeometric distribution analysis without multiple correction adjustment. **c**,**d**, Expression of genes that comprise ECM organization (**c**) and muscle contraction (**d**) gene ontology terms upregulated in *TV-Dhet* cardiomyocytes are normalized to CTRL cardiomyocytes (white bar). **e**, *VCL* expression levels are decreased in *TV-Dhet* cardiomyocytes compared to CTRL cardiomyocytes. DEseq2-adjusted *P* values displayed for *TV-Dhet* gene expression relative to CTRL cardiomyocytes. Gene expression *P* values were calculated using the Wald test with a Benjamini–Hochberg procedure false discovery rate adjustment. ****$P < 0.0001$. **f**, STRING database analysis reveals protein–protein interactions between the proteins encoded by upregulated genes, TPM1, VCL and limited high-confidence interactors. TPM1 and VCL are predicted to interact with upregulated components of the sarcomere (red oval) and costamere–ECM complex (blue oval), respectively. The darker edges represent increased STRING database interaction confidence.

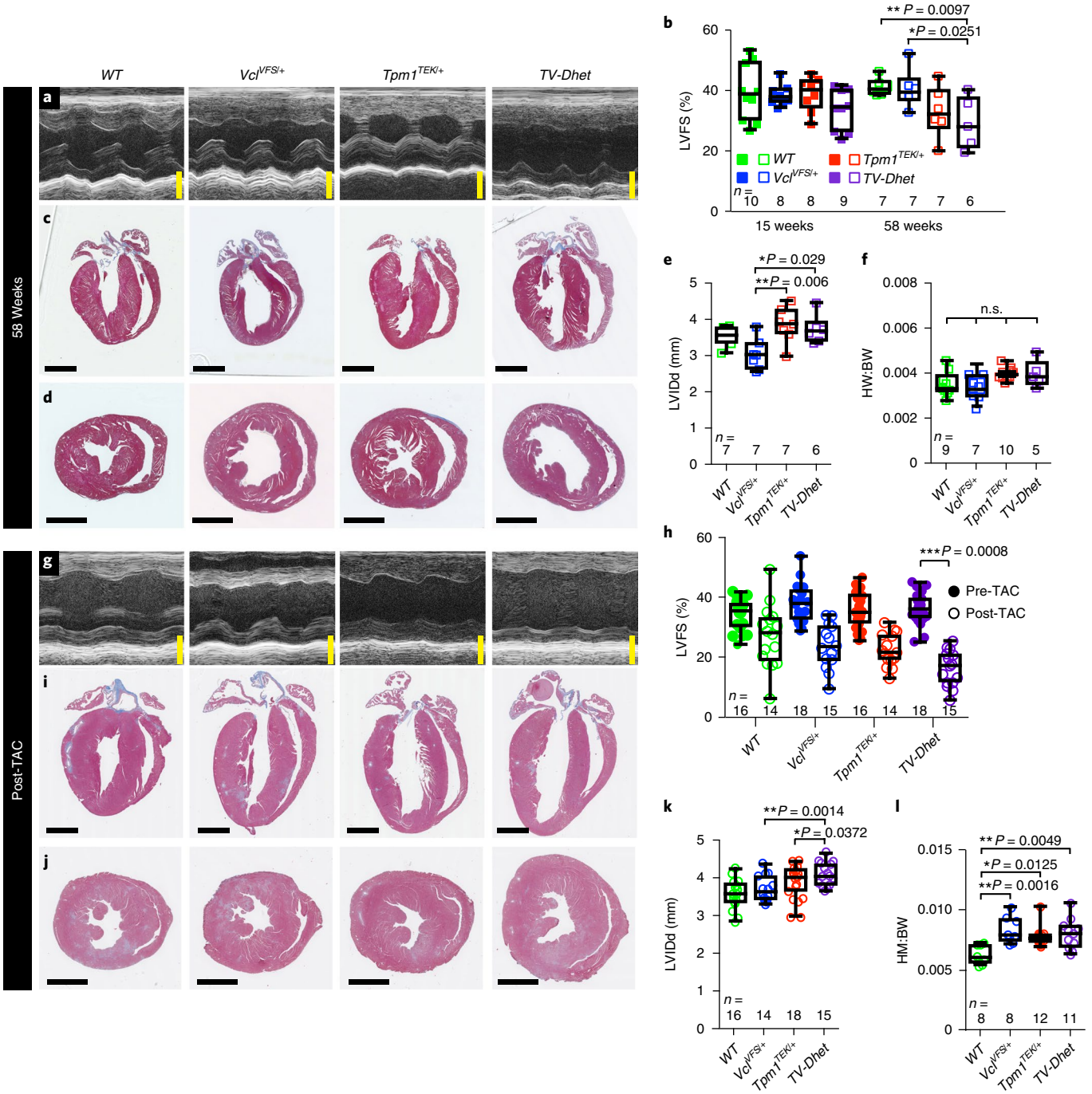

Fig. 4 | *TV-Dhet* mouse hearts exhibit reduced contractility and respond worse than *WT* control mouse hearts to TAC. a,**b**, M-mode echocardiography (**a**) reveals that left-ventricular fractional shortening (LVFS) percentage (**b**), a measure of cardiac function, is decreased in *TV-Dhet* mice compared to *WT* and *Vcl*$^{VFS/+}$ mice at 58 weeks. **c**–**f**, Trichrome sections of mouse hearts (**c**,**d**) and echocardiographic measurements of left ventricular internal dimension in diastole (LVIDd; **e**) reveal that *TV-Dhet* mouse hearts are not significantly dilated compared to *WT*; in addition, the heart-to-body-weight ratios (HW:BW; **f**) do not differ significantly between genotypes at 58 weeks. In **b**,**e** and **f**, filled and open squares indicate 15 and 58 week timepoints, respectively. **g**,**h**, M-mode echocardiography of pre-TAC (14–16 weeks) and (**g**) post-TAC (one week following TAC surgery) mouse hearts reveals that the LVFS (**h**) is significantly reduced in *TV-Dhet* post-TAC mice when compared with *WT* post-TAC mice. **i**–**k**, Trichrome sections and LVIDd measurements of post-TAC mouse hearts show increased chamber size in *TV-Dhet* mice compared with *WT* mice. **l**, Post-TAC heart-to-body-weight ratios are also increased in mice with *TEK* and/or *VFS* variants compared to *WT* mice. Data are presented as interquartile range (box), around the mean (horizontal line), with whiskers representing the minimum and maximum of the dataset, with the individual data points superimposed. $^{*}P < 0.05$; $^{**}P < 0.01$; $^{***}P < 0.001$; n.s., no statistically significant comparisons; one-sided ANOVA with Tukey multiple correction test alpha. *n*, number of biologically independent mice of each genotype used for each study. Scale bars, 2 mm. The complete echocardiography data are available in Supplementary Tables 6 and 7.

(Fig. 1 and Table 1), we further investigated the function of these *TEK* and *VFS* variants in mouse models where DCM can be examined at the organ level. To this end, we employed CRISPR genome-editing strategies to create isogenic C57BL/6J mice carrying these patient-specific *TEK* and *VFS* variants (Supplementary Fig. 7), which were confirmed for targeting specificity as previously

reported (Supplementary Table 4)[15]. Similar to our findings in human *TV-Dhet* fibroblasts (Supplementary Fig. 2), $Vcl^{VFS/+}$ and *TV-Dhet* mouse myocardium exhibited reduced Vcl protein levels, predominantly of the Vcl rather than meta-vinculin isoform, with no evidence of truncated Vcl peptide translation (Supplementary Fig. 8). Furthermore, $Vcl^{VFS/+}$ and *TV-Dhet* mice were viable and without any obvious baseline phenotypes. Supporting that the *VFS* variant produces a true loss-of-function allele, $Vcl^{VFS/VFS}$ mice were embryonically lethal, phenocopying homozygous *Vcl* knockout mice as previously reported (Supplementary Fig. 9)[24]. On the other hand, both $Tpm1^{TEK/+}$ and $Tpm1^{TEK/TEK}$ mice were viable, but at 58 weeks of age $Tpm1^{TEK/TEK}$ mice exhibited significantly decreased cardiac contractility, thus indicating that the *TEK* variant is also pathologically relevant (Supplementary Fig. 10 and Supplementary Table 5).

To examine the in vivo effects of heterozygous *TEK* and *VFS* variants on mouse cardiac function, we analysed left ventricular contractility, chamber dimension and wall thickness in $Tpm1^{TEK/+}$, $Vcl^{VFS/+}$ and *TV-Dhet* mouse hearts by echocardiography and histology (Fig. 4a–e and Supplementary Table 6). Consistent with data from our family cohort, *TV-Dhet* mice, but not $Tpm1^{TEK/+}$ or $Vcl^{VFS/+}$ mice, exhibited significantly decreased left ventricular contractility compared to wild-type (WT) mice at 58 weeks (Fig. 4b); however, these *TV-Dhet* mice did not display ventricular dilation, increased diastolic wall thickness or significant change in heart-to-body-weight ratios (Fig. 4c–f and Supplementary Table 6), which suggests that additional factors may synergize with *TV-Dhet* variants to contribute to the severity of the DCM phenotype. Thus, given that *TV-Dhet* variants exhibit not only variable DCM penetrance and expressivity in our human family cohort (Fig. 1 and Table 1), but also modest pathologic cardiac effects in isogenic mouse models, we further investigated whether haemodynamic stress may mediate disease susceptibility in this complex genetic background by subjecting mouse hearts to transverse aortic constriction (TAC). This form of haemodynamic stress can increase cardiac workload similar to that observed in hypertension or other cardiac diseases, such as valvular stenosis[25]. To this end, *TV-Dhet*, $Tpm1^{TEK/+}$, $Vcl^{VFS/+}$ and WT mice were subjected to TAC or sham surgery (control) and then examined by echocardiography after one week. No significant change in contractility was detected in any of the sham-operated mice (Supplementary Fig. 11 and Supplementary Table 7), but hearts exposed to TAC for one week (post-TAC) displayed decreased cardiac contractility when compared to left ventricular function before TAC (pre-TAC; Fig. 4g,h and Supplementary Table 7). Most importantly, *TV-Dhet* post-TAC hearts displayed significantly worse contractility than WT post-TAC hearts and, notably, the $Tpm1^{TEK/+}$ and $Vcl^{VFS/+}$ hearts also showed a decrease in contractility that was intermediate between *TV-Dhet* and WT hearts (Fig. 4h and Supplementary Movies 1–8). Supporting the notion that haemodynamic stress affects the impact of *TEK* and *VFS* variants on the DCM phenotype, we observed that post-TAC *TV-Dhet* hearts also exhibited left-ventricular dilation and cardiac hypertrophy (Fig. 4i–l and Supplementary Table 7), in contrast to the unstressed *TV-Dhet* hearts that only displayed reduced contractility with ageing. Despite these functional differences, histopathologic studies revealed no significant difference in cardiomyocyte size or myocardial fibrosis between genotypes at 58 weeks of age or subsequent to TAC or sham surgery (Supplementary Fig. 12). Overall, these results not only confirm the pathogenicity of the *TEK* and *VFS* variants in vivo but also support the cooperative interactions of potentially deleterious genetic variants with disease stressors, which together may influence the penetrance and expressivity of DCM.

Discussion

Utilizing a combination of human genetic studies, patient-derived hiPSCs, and genome-edited hESC and mouse models, we provide evidence supporting the interplay between genetic variants and disease stressors in the aetiology of cardiac disease. These results may account for elements of the missing heritability of DCM observed in studies of population genetics[1,26,27]. Although previous studies have reported individual *TPM1* and *VCL* genetic variants as associated with various cardiomyopathies[3,11], we provide functional evidence that genetic variants in these sarcomeric and costameric genes may act synergistically to lead to DCM. Experimental interrogation of these *TPM1* and *VCL* alleles in both hPSC cardiomyocyte and mouse models supports the idea that these alleles may exhibit gene dosage effects whereby homozygous alleles display more severe phenotypes, including embryonic lethality, but heterozygous alleles alone have more modest effects, which may only manifest as pathological when present in combination with other genetic variants and/or disease stressors. These findings may explain why homozygous alleles of these variants have not been observed in exome databases[28] or in our pedigree.

This work further emphasizes how genetic variants can have compound effects that may be further influenced by other disease stressors and may explain the variable penetrance and expressivity in many cases of DCM. Thus, combinatorial genetic alterations in cardiac proteins may not only cooperate to regulate cardiomyocyte force generation and transmission, such as those caused by alterations in the sarcomeric protein TPM1 and the costameric protein VCL, but also increase the susceptibility to overt cardiomyopathies when an additional insult, whether genetic and/or environmental, is superimposed on defects in these pathways. As more genetic variants are discovered through whole-exomic and genomic sequencing of large numbers of patients, interactome pathway models may be valuable in ascertaining whether sequence variants in various cardiac genes may synergistically interact to lead to disease (Fig. 3). Furthermore, information on how biophysical forces impact these interactomes may provide insight into how stresses, such as hypertension or other cardiovascular disorders, can interact with genetic variants to cause cardiomyopathies[1,29]. Overall, these results illuminate how compound genetic interactions can synergistically result in cardiomyopathies and, moreover, corroborate that modifying disease or environmental factors may notably alter genetic risk to cardiomyopathies as was recently suggested for coronary artery disease[30].

Methods

Patient sequencing and clinical data collection. Informed written consent was obtained from all family members who were genetically tested. Permission to release protected health information from clinical records was obtained from all patients or their legal representatives. Disease status assignment and phenotyping was determined by patient self-reporting and clinical diagnoses made by echocardiography or coroner reports. Saliva samples were collected and genomic DNA (gDNA) was purified using the QIAamp DNA Blood Mini Kit (Qiagen, 51104). PCR amplification (Supplementary Table 8) of a targeted region surrounding the *TPM1* c.97G>A and *VCL* c.659dupA alleles was performed using LongAmp Taq DNA Polymerase (NEB, M0323S) per the manufacturer's instructions. Amplicons were gel extracted (Qiagen, 28706) and Sanger sequenced. The ages reported in the pedigree were the ages of individuals at the time of genetic sequencing in this study.

Human cardiac histology. Patient and control left-ventricular free wall samples were fixed with 4 or 37% formaldehyde and paraffin embedded for sectioning. Sections were stained with haematoxylin and eosin or trichrome stains by the University of California San Diego (UCSD) Histology and Immunohistochemistry Core facility and were imaged using a Hamamatsu Nanozoomer 2.0HT Slide Scanner (Hamamatsu Photonics).

Statistical genetic analyses. A kinship matrix (directly related genetic relationship matrix) was derived from the pedigree using the kinship2 R package[31]. Mixed linear model association analysis was then performed by incorporating the kinship matrix using functions from the genetic analysis and the generalized linear model R packages[32]. The effect size of the association between genotype and phenotype is reported as beta ± s.e. The associated *P* values were corrected for the number of genes analysed. Fisher's exact test *P* values and odds ratios with 95% CIs were calculated using the phenotype (clinical diagnosis of cardiomyopathy or not) from all genotyped family members.

Linkage analysis was performed using gDNA isolated from selected individuals from whom sufficient, high-quality gDNA was available. Illumina HumanCoreExome-12 v1-1 BeadChip arrays were used to determine DNA sequence at >500k single nucleotide variants in these samples as per the manufacturer's instructions. The MERLIN v1.1.2 software package was used to calculate non-parametric ExLOD scores that were plotted in R as previously described[33,34]. If any variants in the cohort subset were shared by all obligate carriers and affected subjects but no unaffected individuals (Theta = 0), a significant non-parametric logarithm of the odds (LOD score) of 3.3 would be calculated. Power analysis was calculated using the Genetic Power Calculator module for case-control for discrete traits[35] with the following settings: high risk allele frequency, 0.3636; prevalence, 0.3636; genotype relative risk, 150; D-prime, 0.9; marker allele frequency, 0.32258; cases, 3; control:case ratio, 2.667 and type one error rate, 0.05, yielding a type two error rate (power) of 0.8. This analysis correlates to an 80% power to detect linkage disequilibrium with significance of $P < 0.05$. B allele frequency (BAF) and log R ratio (LRR) statistics were also calculated using MERLIN v1.1.2 analysis of single nucleotide variant arrays and were plotted using custom R scripts to display diploid genome heterozygosity across the autosomes of analysed family members.

Fibroblast cell culture and qRT–PCR. Human fibroblasts were obtained from a punch biopsy and cultured in Dulbecco's Modified Eagle's medium supplemented with 10% fetal bovine serum as previously described[36]. Cycloheximide was administered for 3 h at 100 μg ml^{-1} as previously described[36,37]. RNA was isolated with TRIzol Reagent (Life Technologies, 15596-018). Complementary DNA was generated using iScript Reverse Transcription Supermix for RT-qPCR (Bio-Rad, 170-8840). Quantitative PCR with reverse transcription (qRT–PCR) was performed using iTaq Universal SYBR Green Supermix (Bio-Rad, 172-5121) and target genes were normalized against the average of three reference genes: *ACTB*, *GAPDH* and *PPIG* (Supplementary Table 8). Relative mRNA levels were calculated using the delta-delta C_T quantification method with the Bio-Rad CFX 3.1 software. The fibroblast cell lines were morphologically confirmed as fibroblasts and confirmed by sequence analysis to be both human and reference sequenced at *VCL* and *TPM1* variant loci. Fibroblast lines were regularly tested for mycoplasma contamination using mycoplasma specific PCR primers (Supplementary Table 8).

Protein conservation and molecular modelling. Conservation alignment was performed using Clustal Omega (http://www.ebi.ac.uk/Tools/msa/clustalo/). Molecular structure representations of the surface charge of TPM1 were generated with PyMOL v1.8 (www.pymol.com) using the structure of TPM1 published by Whitby and colleagues (Protein Data Bank/PDB ID number for TPM1: 1C1G)[13].

CRISPR–Cas9 genomic editing of hESCs, hiPSC generation and hESC/hiPSC pluripotency characterization. Human embryonic stem cells (WiCell, WA09) and hiPSCs were maintained in a feeder-free system on Matrigel-coated tissue culture plates (BD Biosciences) in mTeSR medium (Stem Cell Technologies). To analyse human variants in an isogenic background, hESCs were edited using the CRISPR–Cas9 system as previously described[38,39]. Targeting gRNA sequences (Supplementary Table 8) were selected to minimize potential off-target binding[15] and inserted into an empty gRNA cloning vector (Addgene, plasmid no. 41824). The gRNA plasmid (50 μg ml^{-1}) and human-codon-optimized Cas9 nuclease (hCas9) plasmid (25 μg ml^{-1}; Addgene, plasmid no. 41815) were introduced into hESCs by electroporation via an Amaxa Nucleofector (program B16) using a human Stem Cell Nucleofector Kit 2 (Lonza). To introduce the patient-specific TEK mutation into the cells, a single-stranded DNA oligonucleotide (1 nmol) containing the *TEK* substitution (Supplementary Table 8) was also included during the nucleofection reaction. Single cells were sorted into 96-well plates using a FACSAria II (BD Biosciences), expanded and genotyped by Sanger sequencing of genomic DNA and PCR clones. Computationally predicted putative off-target CRISPR-target gRNA sites were PCR amplified from gDNA of hESC lines and Sanger sequenced to verify homology with unedited lines as previously described[15]. *VCL*$^{VFS1/+}$ hESCs were tested for evidence of *VCL* mRNA nonsense-mediated decay using cycloheximide treatment and qRT–PCR protocols as described above for human fibroblasts.

Sendai virus reprogramming of human fibroblasts was used to generate hiPSC lines as previously described as part of the iPSCORE project[14]. The hiPSC and CRISPR-edited hESC lines were fixed with 3.7% formaldehyde, nuclear stained with Hoechst 33352 (1:2,000; ThermoFisher Scientific) and analysed by immunofluorescence for pluripotency markers including POU5F1 (OCT4; 1:100; Abcam, ab27985), NANOG (1:20; Abgent, AP1486c) and SOX2 (1:100; Abcam, ab171380). The following conjugated secondary antibodies were used (all 1:1,000, ThermoFisher Scientific): anti-mouse IgG Alexa Fluor 488 (A21202), anti-rabbit IgG Alexa Fluor 568 (A10042) and anti-goat IgG Alexa Fluor 647 (A21447). Cardiomyocytes (hiPSC and hESC) were analysed for maturity levels by qRT–PCR analysis of MYH7 and MYH6 as previously described[40]. The primer sequences are presented in Supplementary Table 8. The hESC and hiPSC lines were regularly tested for mycoplasma contamination using mycoplasma specific PCR primers (Supplementary Table 8).

Differentiation of hPSCs into cardiomyocytes. Directed differentiation of hPSCs to cardiomyocytes was carried out using established protocols[16], followed by metabolic purification for cardiomyocyte enrichment[17]. At differentiation day 50, cells were dissociated with TrypLE Express (Gibco) and fixed with 1% formaldehyde followed by 90% cold methanol. Cells were washed with PBS containing 2.5% goat serum and 1% Triton-X100 (Flow Buffer) and incubated in primary antibodies against α-muscle actin (1:100; Abcam, ab32575) and cardiac troponin T (1:100; ThermoFisher Scientific, MS-295-P). Cells were washed, incubated with Alexa Fluor 488 and Alexa Fluor 633 (ThermoFisher Scientific, A21070) antibodies and washed again in Flow Buffer. Cell protein expression was analysed using an LSRFortessa flow cytometer (BD Biosciences). Directed cardiac differentiation efficiency was calculated as the percentage of cells expressing both smooth muscle actin and cardiac troponin T, as previously described[16].

Traction force microscopy. The contractility of hPSC cardiomyocytes was assessed using traction force microscopy according to established protocols[41]. Compliant polyacrylamide culture substrates embedded with fluorescent microbeads were polymerized onto 35-mm-glass-bottom culture dishes (Matek). In brief, the glass surface was activated with ultraviolet/ozone and functionalized with 20 mM 3-(trimethoxysilyl)-propylmethacrylate (Sigma-Aldrich) to enable covalent attachment of the polyacrylamide hydrogel. Polymerization was carried out with a solution of 10% acrylamide, 0.1% N,N′-methylenebisacrylamide, 1% ammonium persulfate, 0.1% N,N,N′,N′-tetramethylethylenediamine and 2% 1.0 μm microspheres (580/605 nm; Invitrogen, F13083) to result in a compliant hydrogel with an elastic modulus of 12 kPa[42]. Polyacrylamide substrates were then functionalized with N-sulphosuccinimidyl-6-(4′-azido-2′-nitrophenylamino) hexanoate to enable covalent attachment of collagen type I (100 μg ml^{-1}; BD Biosciences).

At differentiation day 50, cardiomyocytes were dissociated with TrypLE Express and re-plated onto polyacrylamide hydrogels at a density of 25,000 cells cm^{-2}. After a five-day recovery period, traction force microscopy was performed using a Nikon Eclipse Ti-S inverted fluorescence microscope with a BD Carv II camera and a stage-top incubator system (Pathology Devices). With a ×60 objective, videos of the fluorescent bead movement were collected at 9.5 frames s^{-1} for a total of 120 frames. The bead movement during cardiomyocyte contraction was analysed using particle image velocimetry as previously described[43] and cardiomyocyte contractility was reported as the mean peak strain energy averaged across all beats recorded in each video. For each cell line, between 44 and 51 cells across at least five different cardiomyocyte differentiations were analysed.

Sarcomere organization analysis. At differentiation day 50, hESC and hiPSC cardiomyocytes were dissociated with TrypLE Express and re-plated at a density of 80,000 cells cm^{-2} on gelatin-coated glass coverslips. After 5 d (differentiation day 55), cells were fixed with 3.7% formaldehyde solution, blocked and permeabilized in PBS containing 5% goat serum and 0.1% Triton-X100, and incubated in primary antibody against α-actinin (1:800; Sigma-Aldrich, A7811). The cells were then washed and incubated with Alexa Fluor 488 (1:1,000) and Hoechst 33352 (1:2,000). For each cell line, 19–26 randomly selected cardiomyocytes were imaged with a ×60 objective. Using a custom ImageJ routine, images were background subtracted, binarized and ten random regions in the cell were assigned for analysis. Fast Fourier transform (FFT) analysis was employed to analyse sarcomere organization as previously described[22]. Briefly, a fast Fourier transform was performed on intensity values from each region and the resulting power spectra were normalized to a value of one. The height of the first non-zero frequency term was used to estimate the sarcomere organization index. All sarcomere organization indices were normalized to the highest recorded value, such that the reported organization index is a value that falls between 0 and 1.

RNA-seq data analysis. At differentiation day 55, hiPSC cardiomyocytes ($n = 3$ biological replicates of independent differentiations from both familial control and *TV-Dhet* iPSCs) were lysed in TRIzol and RNA was extracted according to the manufacturer's instructions. RNA libraries were prepared using the Illumina TruSeq RNA Library Prep Kit and sequenced using the Illumina HiSeq 4000 system to generate 50 bp single-end reads. FastQC (http://www.bioinformatics.babraham.ac.uk/projects/fastqc) and dupRadar tools were used to assess read quality[44]. Reads were aligned using Kallisto[45] to transcripts from GENCODE v.25 excluding transcripts from the Y chromosome[46]. Gene counts were generated from transcript counts using the tximport R package[47]. Genes with low expression counts (<100) were excluded and differential expression levels among the remaining genes were calculated using the DESeq2 R package[48] with the following significance criteria: expression fold change <0.8 or >1.2 and $P < 0.01$, calculated using a Wald test with a Benjamini–Hochberg procedure false discovery rate adjustment[22]. Clustergram analysis was performed with differentially expressed genes using the pheatmap R package. Gene ontology term analysis was performed on differentially expressed genes using metascape (http://metascape.org)[49]. Proteins encoded by genes comprising selected gene ontology terms were investigated using STRING network (v10.5) analysis with TPM1, VCL and limited ($n = 5$) high-confidence interactors to create a predicted protein–protein interactome network[23]. *TITIN* N2BA and *VCL* exon splice isoform inclusion ratios were calculated from RNA-seq transcripts that were mapped using STAR v2.5.2b[50] to the hg19

reference genome. Alternative splicing events for mRNA expression in familial control (CTRL) and *TV-Dhet* hiPSC cardiomyocytes were quantified using rMATS v3.2.5 and the default parameters[51] with a false discovery rate of less than 0.05 considered significant.

Mouse CRISPR-mediated genomic editing, genotyping and colony maintenance. CRISPR-targeting constructs were injected into C57BL/6NHsd single cell zygotes (Harlan Sprague Dawley Inc.) by the UCSD Transgenic Mouse Core Facility as previously described[52,53]. The injection mix contained 20 ng μl^{-1} guide RNA (gRNA), 50 ng μl^{-1} *Cas9* mRNA and 100 ng μl^{-1} single-stranded DNA repair oligonucleotide. Sequences targeting gRNA (Supplementary Table 8) were selected to minimize potential off-target nuclease activity[15]. Tail clips were taken to isolate gDNA for genotyping. The top ten predicted off-target sites in F_0 founder mouse genomes were analysed for evidence of non-specific nuclease activity by targeted amplification and Sanger sequencing[15]. Mice were outcrossed to WT C57BL/6 mice for at least six generations and were genotyped by either Sanger sequencing of the target loci or by allele-specific PCR. All analysed mice were male and between 15 and 59 weeks of age.

Mouse embryonic lethality studies. Heterozygous *Tpm1*$^{TEK/+}$ or *Vcl*$^{VFS/+}$ mice were incrossed and the resultant litters were genotyped. Because no *Vcl*$^{VFS/VFS}$ mice were identified at birth across multiple litters, timed *Vcl*$^{VFS/+}$ sibling matings were performed and pregnant mice were dissected between embyonic day 9.5 and 13.5 (E9.5 and E13.5) as previously described[24]. The resultant embryos were assigned a unique identifier, photographed, collected and genotyped.

Echocardiography and transverse aortic constriction. Mouse echocardiography was performed as previously described[54]. Briefly, hair removal cream was used to expose the anterior chest wall and mice were anaesthetized with 5% isoflurane induction and 0.5% isoflurane maintenance. Transthoracic echocardiography (M-mode and two-dimensional) was performed using a Vevo 2100 (VisualSonics Inc.) high-frequency ultrasound instrument with simultaneous electrocardiogram acquisition via small-needle electrodes. The heart rate was maintained above 500 beats per minute and body temperature was maintained using a warming station. Researchers blinded to mouse genotypes measured the heart rate, left ventricular internal dimension during diastole and systole (LVIDd/s), end-diastolic interventricular septal thickness in diastole and left ventricle posterior wall thickness in diastole from echocardiographic recordings. Left ventricular fractional shortening percentage, a measure of cardiac contractility, was calculated as the average of three (LVIDd−LVIDs)/LVIDd measurements per animal; $n = 6$–14 mice per group in ageing studies.

TAC was performed as previously described[25,54]. Briefly, 12- to 16-week-old male mice were anaesthetized with an intraperitoneal injection of ketamine (100 mg kg^{-1}) and xylazine (10 mg kg^{-1}), intubated and connected to a mouse ventilator (Harvard). Following a small incision in the second intercostal space at the left upper sternal border, a double blunted 27-gauge (for mice over 25 g) or 27.5-gauge needle (for mice below 25 g) was ligated to the aorta between the innominate and left common carotid arteries using a 7-0 silk suture. The needle was then removed and the chest wall and skin were sutured closed. Sham surgery mice underwent all components of the TAC surgery, including anaesthesia, intubation, chest wall incision and incision closure, except for aortic suture ligation. Repeat transthoracic echocardiography was performed one week after surgery.

At study termination, systolic pressure gradients were measured by selective cannulation of the left and right carotid arteries; the pressure wave form was recorded (average pressure gradients greater than 70 mm Hg per genotype) and heart tissue was collected for histological and protein analyses; $n = 14$–18 mice per genotype in the TAC studies, $n = 5$ or 6 mice per genotype in the sham control surgeries.

Morphometric analyses and histology. Animals were anaesthetized with ketamine/xylazine and euthanized at 58 weeks of age or one week following TAC or sham surgery in accordance with IACUC protocols. Mice and collected hearts were weighed to calculate heart-weight-to-body-weight ratios (mg mg^{-1}—arbitrary units). In the ageing studies, 5–10 animals were analysed per genotype; 8–12 animals per genotype were analysed in TAC surgery conditions and five or six animals per genotype were analysed in sham surgery conditions. Hearts were fixed with 4% paraformaldehyde, dehydrated in 70% ethanol and embedded in paraffin. Paraffin-embedded cardiac sections (8-μm thick) were trichrome stained at the UCSD Histology and Immunohistochemistry Core facility and were imaged using a Hamamatsu Nanozoomer 2.0HT Slide Scanner. Trichrome-positive regions of mouse heart sections were quantified as a percentage of total cardiac cross-sectional area using ImageJ software ($n = 3$ or 4 in 58 week mice, $n = 4$ in post-sham mice, $n = 7$–10 in post-TAC mice). Mouse cardiac-papillary-muscle sections, fixed in 4% paraformaldehyde and embedded in optimal cutting temperature compound, were cryosectioned at a thickness of 7 μm, washed in PBS and stained with Alexa Fluor 488 conjugated wheat germ agglutinin (ThermoFisher, W11261) at 5 μg ml^{-1} and DAPI at 0.1 μg ml^{-1}. Cell outlines were measured using Image Pro Plus 6.0 software (Media Cybernetics) and averaged to determine the average cardiomyocyte cross-sectional area (μm^2; $n = 3$ mice and 100 cardiomyocytes per genotype, for each condition).

Protein preparation and western blot analysis. Fibroblast and hESC/hiPSC pellets were harvested and lysed in protein lysis buffer (50 mM Tris–HCl pH 7.4, 150 mM NaCl, 1 mM EGTA, 1 mM EDTA, 1% NP-40 and protease inhibitor (Amresco)). Total protein was isolated from mouse hearts in heart lysis buffer (10 mM Tris–HCl, pH 8, 100 mM NaCl, 1% NP-40, 2 mM sodium orthovanadate and protease inhibitor (Roche Applied Science)). Protein lysates were quantitated using a Qubit Protein Assay (Life Technologies, Q33211). Lysates underwent gel electrophoresis on a 10–20% Tris glycine SDS–PAGE gel (Novex; EC6135), which was then transferred to polyvinylidene difluoride membrane (Immobilon; IPVH0010) for immunoblotting. Blots were blocked in 5% milk in Tris-buffered saline with 1% Tween (TBST), incubated with primary antibody in 5% milk in TBST, washed in TBST and imaged using Clarity Western ECL substrate (Bio-Rad, 170-5060). The antibodies used include: anti-vinculin (Sigma, V9131), anti-N-terminal vinculin (Santa Cruz Biotechnology, sc-5573), anti-tropomyosin 1 (Abcam, EPR5159), anti-tubulin (Sigma, T5168) and anti-GAPDH (GeneTex, GTX100118 or Santa Cruz Biotechnology; sc-32233). Densitometric protein quantitation was performed using Bio-Rad ImageLab 5.0 or ImageJ software. At least three replicates were performed per quantitation and average density was compared by Student's *t*-test or ANOVA as appropriate.

Statistical analysis. All data compared in statistical analyses were collected from experiments conducted at least three times with reproducible results. All statistical analyses were performed on measurements of at least three independent biologic replicates. Protein quantitation was performed on a minimum of three technical and three biological replicates per sample. Data were expressed as mean ± s.e.m., except where otherwise noted. Comparison of data sets was performed using Student's *t*-tests with two-sided analysis or ordinary one-way ANOVA analysis with Tukey multiple correction tests, as appropriate for data type. Differences between mean values were considered to be significant when $P < 0.05$. Gene-expression value comparisons were performed using the Wald test with Benjamini–Hochberg procedure false discovery rate adjustment. Previous experimental results in comparable systems were used to determine sample sizes for cell culture and mouse experiments. The analysis of traction force microscopy and echocardiography measurements was performed by researchers blinded to sample genotype. No data were excluded, except as described in the RNA-seq analysis methods.

Study approval. ll human study protocols were approved by the UCSD Institutional Review Board and Human Research Protections Program and written informed consent was obtained from all study participants (Protocol no. 111523). Collection of skin fibroblasts was performed with IRB approval (Protocol nos 110776, 111475 and 090243). The use of human-derived pluripotent cells in this study was approved by the UCSD Institutional Review Board and Embryonic Stem Cell Research Oversight Committee (Protocol nos 141315 and 111475). All animal procedures were performed in accordance with the National Institute of Health guidelines and were approved by the UCSD Institutional Animal Care and Use Committee (Protocol nos S13138 and S00138). UCSD has an Animal Welfare Assurance (no. A3033-01) on file with the Office of Laboratory Animal Welfare and is fully accredited by AAALAC International. All studies reported in this manuscript were performed in compliance with all relevant ethical regulations.

Reporting Summary. Further information on research design is available in the Nature Research Reporting Summary linked to this article.

Code availability

All custom code used in this study can be found at http://github.com/englea52/Englerlab or https://github.com/enfarah/digital_karyotype.

Data availability

The authors declare that all data supporting the findings of this study are available within the paper and its Supplementary Information. The materials and data of this study are available from the corresponding author on reasonable request, with the exception of patient DNA and tissue, which is limited and protected by local and federal privacy regulations. Microarray study and RNA-seq data are available via dbGaP with GEO accession numbers GSE121844 and GSE121559.

Received: 14 September 2017; Accepted: 7 January 2019;
Published online: 7 February 2019

References

1. Hershberger, R. E., Hedges, D. J. & Morales, A. Dilated cardiomyopathy: the complexity of a diverse genetic architecture. *Nat. Rev. Cardiol.* **10**, 531–547 (2013).
2. Benjamin, E. J. et al. Heart disease and stroke statistics—2017 update: a report from the American Heart Association. *Circulation* **135**, e146–e603 (2017).

3. Stenson, P. D. et al. The Human Gene Mutation Database: towards a comprehensive repository of inherited mutation data for medical research, genetic diagnosis and next-generation sequencing studies. *Hum. Genet.* **136**, 665–677 (2017).
4. Villard, E. et al. A genome-wide association study identifies two loci associated with heart failure due to dilated cardiomyopathy. *Eur. Heart J.* **32**, 1065–1076 (2011).
5. Meder, B. et al. A genome-wide association study identifies 6p21 as novel risk locus for dilated cardiomyopathy. *Eur. Heart J.* **35**, 1069–1077 (2014).
6. Li, L., Bainbridge, M. N., Tan, Y., Willerson, J. T. & Marian, A. J. A potential oligogenic etiology of hypertrophic cardiomyopathy: a classic single gene disorder. *Circ. Res.* **126**, 1084–1090 (2017).
7. Roncarati, R. et al. Doubly heterozygous LMNA and TTN mutations revealed by exome sequencing in a severe form of dilated cardiomyopathy. *Eur. J. Hum. Genet.* **21**, 1105–1111 (2013).
8. Maron, B. J., Maron, M. S. & Semsarian, C. Double or compound sarcomere mutations in hypertrophic cardiomyopathy: a potential link to sudden death in the absence of conventional risk factors. *Heart Rhythm* **9**, 57–63 (2012).
9. Petropoulou, E. et al. Digenic inheritance of mutations in the cardiac troponin (TNNT2) and cardiac beta myosin heavy chain (MYH7) as the cause of severe dilated cardiomyopathy. *Eur. J. Med. Genet.* **60**, 485–488 (2017).
10. Haas, J. et al. Atlas of the clinical genetics of human dilated cardiomyopathy. *Eur. Heart J.* **36**, 1123–1135 (2014).
11. Kimura, A. Molecular genetics and pathogenesis of cardiomyopathy. *J. Hum. Genet.* **61**, 41–50 (2016).
12. Olson, T. M., Kishimoto, N. Y., Whitby, F. G. & Michels, V. V. Mutations that alter the surface charge of alpha-tropomyosin are associated with dilated cardiomyopathy. *J. Mol. Cell. Cardiol.* **33**, 723–732 (2001).
13. Whitby, F. G. & Phillips, G. N. Crystal structure of tropomyosin at 7 Angstroms resolution. *Proteins* **38**, 49–59 (2000).
14. Panopoulos, A. D. et al. iPSCORE: a resource of 222 iPSC lines enabling functional characterization of genetic variation across a variety of cell types. *Stem Cell Rep.* **8**, 1086–1100 (2017).
15. Hsu, P. D. et al. DNA targeting specificity of RNA-guided Cas9 nucleases. *Nat. Biotechnol.* **31**, 827–832 (2013).
16. Lian, X. et al. Directed cardiomyocyte differentiation from human pluripotent stem cells by modulating Wnt/β-catenin signaling under fully defined conditions. *Nat. Protoc.* **8**, 162–175 (2013).
17. Tohyama, S. et al. Distinct metabolic flow enables large-scale purification of mouse and human pluripotent stem cell-derived cardiomyocytes. *Cell Stem Cell* **12**, 127–137 (2012).
18. Dhalla, A. K., Hill, M. F. & Singal, P. K. Role of oxidative stress in transition of hypertrophy to heart failure. *J. Am. Coll. Cardiol.* **28**, 506–514 (1996).
19. Rosenkranz, S. et al. Alterations of β-adrenergic signaling and cardiac hypertrophy in transgenic mice overexpressing TGF-β_1. *Am. J. Physiol. Heart Circ. Physiol.* **283**, H1253–H1262 (2002).
20. Razeghi, P. et al. Metabolic gene expression in fetal and failing human heart. *Circulation* **104**, 2923–2931 (2001).
21. Bristow, M. R. et al. β1- and β2-adrenergic-receptor subpopulations in nonfailing and failing human ventricular myocardium: coupling of both receptor subtypes to muscle contraction and selective β1-receptor down-regulation in heart failure. *Circ. Res.* **59**, 297–309 (1986).
22. Hinson, J. T. et al. HEART DISEASE. Titin mutations in iPS cells define sarcomere insufficiency as a cause of dilated cardiomyopathy. *Science* **349**, 982–986 (2015).
23. Szklarczyk, D. et al. STRINGv10: protein–protein interaction networks, integrated over the tree of life. *Nucleic Acids Res.* **43**, D447–D452 (2015).
24. Xu, W., Baribault, H. & Adamson, E. D. Vinculin knockout results in heart and brain defects during embryonic development. *Development* **125**, 327–337 (1998).
25. Rockman, H. A. et al. Segregation of atrial-specific and inducible expression of an atrial natriuretic factor transgene in an in vivo murine model of cardiac hypertrophy. *Proc. Natl Acad. Sci. USA* **88**, 8277–8281 (1991).
26. Golbus, J. R. et al. Population-based variation in cardiomyopathy genes. *Circ. Cardiovasc. Genet.* **5**, 391–399 (2012).
27. McNally, E. M. & Puckelwartz, M. J. Genetic variation in cardiomyopathy and cardiovascular disorders. *Circ. J.* **79**, 1409–1415 (2015).
28. Lek, M. et al. Analysis of protein-coding genetic variation in 60,706 humans. *Nature* **536**, 285–291 (2016).
29. Happe, C. L. & Engler, A. J. Mechanical forces reshape differentiation cues that guide cardiomyogenesis. *Circ. Res.* **118**, 296–310 (2016).
30. Khera, A. V. et al. Genetic risk, adherence to a healthy lifestyle, and coronary disease. *N. Engl. J. Med.* **375**, 2349–2358 (2016).
31. Therneau, T. M. et al. kinship2: pedigree functions v.1.6.4. (CRAN, 2015); https://cran.r-project.org/package=kinship2
32. Marschner, I.C. & Donoghoe, M. W. glm2: fitting generalized linear models v.1.2.1. (CRAN, 2018); https://CRAN.R-project.org/package=glm2
33. Abecasis, G. R., Cherny, S. S., Cookson, W. O. & Cardon, L. R. Merlin—rapid analysis of dense genetic maps using sparse gene flow trees. *Nat. Genet.* **30**, 97–101 (2002).
34. McGregor, T. L. et al. Consanguinity mapping of congenital heart disease in a South Indian population. *PLoS ONE* **5**, e10286 (2010).
35. Purcell, S., Cherny, S. S. & Sham, P. C. Genetic Power Calculator: design of linkage and association genetic mapping studies of complex traits. *Bioinformatics* **19**, 149–150 (2003).
36. Hashem, S. I. et al. Oxidative stress mediates cardiomyocyte apoptosis in a human model of Danon disease and heart failure. *Stem Cells* **33**, 2343–2350 (2015).
37. Carter, M. S. et al. A regulatory mechanism that detects premature nonsense codons in T-cell receptor transcripts in vivo is reversed by protein synthesis inhibitors in vitro. *J. Biol. Chem.* **270**, 28995–29003 (1995).
38. Byrne, S. M., Mali, P. & Church, G. M. in *Methods in Enzymolology*, Vol. 546 (eds Doudna, J.A. & Sontheimer, E.J.) 119–138 (Elsevier, Amsterdam, 2014).
39. Yang, L., Mali, P., Kim-Kiselak, C. & Church, G. CRISPR–Cas-mediated targeted genome editing in human cells. *Methods Mol. Biol.* **1114**, 245–267 (2014).
40. Giacomelli, E. et al. Three-dimensional cardiac microtissues composed of cardiomyocytes and endothelial cells co-differentiated from human pluripotent stem cells. *Development* **144**, 1008–1017 (2017).
41. Wu, H. et al. Epigenetic regulation of phosphodiesterases 2A and 3A underlies compromised β-adrenergic signaling in an iPSC model of dilated cardiomyopathy. *Cell Stem Cell* **17**, 89–100 (2015).
42. Tse, J. R. & Engler, A. J. Preparation of hydrogel substrates with tunable mechanical properties. *Curr. Protoc. Cell BioI.* **47**, 10.16.1–10.16.16 (2010).
43. del Alamo, J. C. et al. Three-dimensional quantification of cellular traction forces and mechanosensing of thin substrata by Fourier traction force microscopy. *PLoS ONE* **8**, e69850 (2013).
44. Sayols, S., Scherzinger, D. & Klein, H. dupRadar: a Bioconductor package for the assessment of PCR artifacts in RNA-Seq data. *BMC Bioinform.* **17**, 428 (2016).
45. Bray, N. L., Pimentel, H., Melsted, P. & Pachter, L. Near-optimal probabilistic RNA-seq quantification. *Nat. Biotechnol.* **34**, 525–527 (2016).
46. Harrow, J. et al. GENCODE: the reference human genome annotation for the ENCODE Project. *Genome Res.* **22**, 1760–1774 (2012).
47. Soneson, C., Love, M. I. & Robinson, M. D. Differential analyses for RNA-seq: transcript-level estimates improve gene-level inferences. *F1000Research* **4**, 1521 (2015).
48. Love, M. I., Huber, W. & Anders, S. Moderated estimation of fold change and dispersion for RNA-seq data with DESeq2. *Genome Biol.* **15**, 550 (2014).
49. Tripathi, S. et al. Meta- and orthogonal integration of influenza "OMICs" data defines a role for UBR4 in virus budding. *Cell Host Microbe* **18**, 723–735 (2015).
50. Dobin, A. et al. STAR: ultrafast universal RNA-seq aligner. *Bioinformatics* **29**, 15–21 (2013).
51. Shen, S. et al. rMATS: robust and flexible detection of differential alternative splicing from replicate RNA-Seq data. *Proc. Natl Acad. Sci. USA* **111**, E5593–E5601 (2014).
52. Yang, H., Wang, H. & Jaenisch, R. Generating genetically modified mice using CRISPR/Cas-mediated genome engineering. *Nat. Protoc.* **9**, 1956–1968 (2014).
53. Wang, H. et al. One-step generation of mice carrying mutations in multiple genes by CRISPR/Cas-mediated genome engineering. *Cell* **153**, 910–918 (2013).
54. Li, R. et al. β1 integrin gene excision in the adult murine cardiac myocyte causes defective mechanical and signaling responses. *Am. J. Pathol.* **180**, 952–962 (2012).

Acknowledgements

We thank the patients who participated in this study. K. DeMali (Univ. Iowa) provided the truncated *Gallus gallus* VCL peptide. Various experiments were conducted with the assistance, expertise and support of the following UCSD core facilities: Institute for Genomic Medicine Core, Mouse Transgenic Core, Histology and Immunohistochemistry Core, Seaweed Canyon Cardiovascular Physiology Laboratory, Microscopy Core and Human Embryonic Stem Cell Core facilities. We also thank P. Mali and H. Taylor-Weiner for assistance with hPSC culture, members of the Bruce Hamilton laboratory for helpful discussions and experimental design and members of the Chi lab for comments on the manuscript. This work was supported in part by grants from the NIH to N.C.C., J.C., R.S.R., E.D.A. and grant no. R01AG045428 to A.J.E. D.C.D. was supported by a CIRM pre-doctoral fellowship (grant no. TG2-01154) and an NIH pre-doctoral training grant (grant no. T32 GM008666). C.L.H. was supported by post-doctoral fellowships from the American Heart Association (grant no. 15POST25720070) and NIH (grant no. F32HL131424). J.C. is an American Heart Association Endowed Chair. E.N.F. was supported by a NIH pre-doctoral training grant (grant no. 4T32HL007444-34).

Author contributions

D.C.D., C.L.H., C.C., A.J.E., R.S.R. and N.C.C. conceived the project. D.C.D., C.L.H., C.C., N.T., A.M.M., T.L., N.D.D., Q.P., E.N.F., Y.G., K.P.T., V.D.T., J.C. and K.L.P. planned the design of studies and conducted experiments. D.C.D. and E.D.A. recruited patients and generated human fibroblast lines. D.C.D. generated CRISPR-edited mouse lines and C.L.H. generated CRISPR-edited hESC lines. Q.P., J.C., K.L.P. and N.J.S. assisted in data interpretation and provided experimental advice. D.C.D., C.L.H., C.C., A.J.E., R.S.R. and N.C.C. prepared and wrote the manuscript.

Competing interests

The authors declare no competing interests.

Additional information

Supplementary information is available for this paper at https://doi.org/10.1038/s41551-019-0348-9.

Reprints and permissions information is available at www.nature.com/reprints.

Correspondence and requests for materials should be addressed to A.J.E., R.S.R. or N.C.C.

Publisher's note: Springer Nature remains neutral with regard to jurisdictional claims in published maps and institutional affiliations.

nature research

Corresponding author(s): Neil Chi, Robert Ross, Adam Engler

Last updated by author(s): Dec 20, 2018

Reporting Summary

Nature Research wishes to improve the reproducibility of the work that we publish. This form provides structure for consistency and transparency in reporting. For further information on Nature Research policies, see Authors & Referees and the Editorial Policy Checklist.

Statistics

For all statistical analyses, confirm that the following items are present in the figure legend, table legend, main text, or Methods section.

n/a	Confirmed
☐	☒ The exact sample size (*n*) for each experimental group/condition, given as a discrete number and unit of measurement
☐	☒ A statement on whether measurements were taken from distinct samples or whether the same sample was measured repeatedly
☐	☒ The statistical test(s) used AND whether they are one- or two-sided *Only common tests should be described solely by name; describe more complex techniques in the Methods section.*
☒	☐ A description of all covariates tested
☐	☒ A description of any assumptions or corrections, such as tests of normality and adjustment for multiple comparisons
☐	☒ A full description of the statistical parameters including central tendency (e.g. means) or other basic estimates (e.g. regression coefficient) AND variation (e.g. standard deviation) or associated estimates of uncertainty (e.g. confidence intervals)
☒	☐ For null hypothesis testing, the test statistic (e.g. *F*, *t*, *r*) with confidence intervals, effect sizes, degrees of freedom and *P* value noted *Give P values as exact values whenever suitable.*
☒	☐ For Bayesian analysis, information on the choice of priors and Markov chain Monte Carlo settings
☒	☐ For hierarchical and complex designs, identification of the appropriate level for tests and full reporting of outcomes
☒	☐ Estimates of effect sizes (e.g. Cohen's *d*, Pearson's *r*), indicating how they were calculated

Our web collection on statistics for biologists contains articles on many of the points above.

Software and code

Policy information about availability of computer code

Data collection	BD FACSDiva software was used to collect flow-cytometry data.
Data analysis	Kinship2, genetic analysis package (GAP), and generalized linear (GLM) R packages were used to perform mixed-linear-model association analyses. MERLIN v1.1.2 software was used to calculate non-parametric ExLOD scores. Power analysis was calculated using the Genetic Power Calculator module for case-control for discrete traits (v.2008). Relative mRNA levels were calculated using the delta-delta CT quantification method using Bio-Rad CFX 3.1 software. Conservation alignment was performed using Clustal Omega (http://www.ebi.ac.uk/Tools/msa/clustalo/). Molecular structure representations of the surface charge of TPM1 were generated with PyMOL v1.8 (www.pymol.com). FlowJo v10 was used to analyze flow cytometry data. For Sarcomere organization analysis, a custom ImageJ routine was used: images were background subtracted, binarized and 10 random regions within the cell were assigned for analysis. Fast Fourier transform (FFT) analysis was employed to analyze sarcomere organization as previously described (PMID: 26315439). RNA-analysis was performed using publicaly available packages from FastQC (v0.11.5) dupRadar (v3.8), Kallisto, the tximport R package, the DESeq2 R package, the pheatmap R package, metascape, and STRING network (v10.5) software. RNA splice isoform analyses were performed using STAR v2.5.2b and quantified using rMATS v3.2.5 with default parameters. Power analysis was calculated using the Genetic Power Calculator module for case-control for discrete traits (http://zzz.bwh.harvard.edu/gpc/cc2.html). For Western Blot densitometry, analysis were performed with Image J (NIH) and Imagelab 5.2.1 (BioRad) software. Echocardiogram analysis was performed with Vevo Lab 2.1.0 (Visualsonics, Inc) software. All statistical analyses were performed using GraphPad Prism Version 6.00 (GraphPad Software, Inc). Cell outlines were measured using Image Pro Plus 6.0 software.

For manuscripts utilizing custom algorithms or software that are central to the research but not yet described in published literature, software must be made available to editors/reviewers. We strongly encourage code deposition in a community repository (e.g. GitHub). See the Nature Research guidelines for submitting code & software for further information.

Data

Policy information about availability of data

All manuscripts must include a data availability statement. This statement should provide the following information, where applicable:

- Accession codes, unique identifiers, or web links for publicly available datasets
- A list of figures that have associated raw data
- A description of any restrictions on data availability

The authors declare that all data supporting the findings of this study are available within the paper and its Supplementary Information. Data and materials used in this study are available from the corresponding author upon reasonable request, with the exception of patient DNA and tissue, which are limited and protected by local and federal privacy regulations. Microarray and RNA-seq data are available via dbGaP with the GEO accession numbers GSE121844 and GSE121559.

Field-specific reporting

Please select the one below that is the best fit for your research. If you are not sure, read the appropriate sections before making your selection.

☒ Life sciences ☐ Behavioural & social sciences ☐ Ecological, evolutionary & environmental sciences

For a reference copy of the document with all sections, see nature.com/documents/nr-reporting-summary-flat.pdf

Life sciences study design

All studies must disclose on these points even when the disclosure is negative.

Sample size	Sample sizes were chosen on the basis of prior similar experiments that used analyses of hiPSC-derived cardiomyocytes (PMID: 26315439) and transverse aortic constriction (TAC), and that took into account expected perioperative and long-term mortality of genetically engineered mouse groups, allowing for clear statistical differences between groups (PMID: 22248583,15331426).
Data exclusions	No data were excluded, except as described in the RNA-seq analysis methods. Transcripts mapped to the Y chromosome were excluded to account for the difference in sex between the proband (TV-Dhet/DCM) and his mother (Control). Genes with low expression counts (<100) were excluded in order to focus on biologically significant variation in gene expression. These exclusion criteria were not pre-established.
Replication	All experiments were repeated at least three times, with comparable results.
Randomization	Littermate controls were used for all mouse experiments. Mice from the groups were randomly assigned for use in either sham or TAC groups. No randomization was performed for human genetic or pluripotent-stem-cell-derived cardiomyocyte analysis as the genetic variation of the samples was known and was the only variable tested. Age of mice and duration of cardiomyocyte culture were matched between groups. No significant covariates existed in colony maintenance or cell culture except as noted for the TAC analysis.
Blinding	Pluripotent-stem-cell-derived cardiomyocyte data collection and analysis was performed while researchers were blinded to cell genotype; genotype was revealed once complete for statistical analyses. Mouse echocardiography experiments were designed and performed in a double-blind manner. The ultrasound technician, the technician performing TAC surgeries, and the researcher measuring echocardiography parameters were blinded to the animal genotypes during experimental-measurement recording, and were only revealed once analysis was complete.

Reporting for specific materials, systems and methods

We require information from authors about some types of materials, experimental systems and methods used in many studies. Here, indicate whether each material, system or method listed is relevant to your study. If you are not sure if a list item applies to your research, read the appropriate section before selecting a response.

Materials & experimental systems

n/a	Involved in the study
☐	☒ Antibodies
☐	☒ Eukaryotic cell lines
☒	☐ Palaeontology
☐	☒ Animals and other organisms
☒	☐ Human research participants
☒	☐ Clinical data

Methods

n/a	Involved in the study
☒	☐ ChIP-seq
☐	☒ Flow cytometry
☒	☐ MRI-based neuroimaging

Antibodies

Antibodies used	Anti-Vinculin (Sigma; Clone: hVIN-1; Cat: V9131; Lot: 034M4809V) and Anti-N-Terminal Vinculin (Santa Cruz Biotechnology; Clone: H-300; Cat: sc-5573; Lot: D1409).

Anti-Tropomyosin 1 (Abcam; Clone: EPR5159; Cat: ab133292; Lot: YH082509).
Anti-GAPDH (Santa Cruz Biotechnology; Clone:6C5;Cat:sc-32233; Lot: B0514).
Anti-Tubulin (Sigma; Clone: B-5-1-2; Cat: T5168, Lot: 118H4899).
Goat polyclonal antibody to Oct4 (Abcam ab27985, Lot no. GR232530-1).
Mouse monoclonal to SOX2 (Abcam ab171380, Lot no. GR161045-2).
Purified Rabbit Polyclonal NANOG Antibody (Abgent AP1486c, Lot no. SH071219F).
Rabbit monoclonal to Alpha Smooth Muscle Actin [E184], (Abcam ab32575, Lot No. GR173883-3).
Anti-Troponin T, Cardiac Isoform Ab-1, Clone: 13-11(MS-295-P Fisher (Thermo Scientific Lab Vision), Lot no. 295P1406C.).
The following conjugated secondary antibodies were used: anti-Mouse IgG Alexa Fluor 488 (A21202), anti-Rabbit IgG Alexa Fluor 568 (A10042), and anti-Goat IgG Alexa Fluor 647 (A21447).

Validation

Anti-Vinculin (Sigma; Clone: hVIN-1; Cat: V9131; Lot: 034M4809V) and Anti-N-Terminal Vinculin (Santa Cruz Biotechnology; Clone: H-300; Cat: sc-5573; Lot: D1409), used for Western Blotting, have been validated previously by our group by testing for background activity in Vinculin knockout mice. Anti-Tropomyosin 1 (Abcam; Clone: EPR5159; Cat: ab133292; Lot: YH082509) has been validated by the manufacturer using human skeletal muscle, human heart, HUVEC, C6, RAW 264.7, PC12 and NIH 3T3 cell lysates; and human muscle tissue. Anti-GAPDH (Santa Cruz Biotechnology; Clone:6C5;Cat:sc-32233; Lot: B0514) – has been validated by the manufacturer using Western blot analysis of GAPDH expression in non-transfected 293T, human GAPDH transfected 293T and Hep G2 whole cell lysates. Anti-Tubulin (Sigma; Clone: B-5-1-2; Cat: T5168, Lot: 118H4899) has been validated by the manufacturer using immunoblotting of extracts of human fibroblasts. Goat polyclonal antibody to Oct4 (Abcam ab27985, Lot no. GR232530-1) Immunogen: Synthetic peptide corresponding to Human Oct4, aa 300 to the C-terminus (C terminal); Vendor website has photographic validations for the performance of immunofluorescence with human cells. Mouse monoclonal to SOX2 (Abcam ab171380, Lot no. GR161045-2); Vendor website has photographic validations for the performance of immunofluorescence with human cells. Purified Rabbit Polyclonal NANOG Antibody (Abgent AP1486c, Lot no. SH071219F); Antigen Region: 94-123 aa; vendor provides validation of the antibody for western blot and ELISA against human samples. Rabbit monoclonal to Alpha Smooth Muscle Actin [E184], (Abcam ab32575, Lot No. GR173883-3), Vendor website image demonstrating the use of this antibody against human cells in flow cytometry. Anti-Troponin T, Cardiac Isoform Ab-1, Clone: 13-11(MS-295-P Fisher (Thermo Scientific Lab Vision), Lot no. 295P1406C.); Vendor datasheet claims antibody is reactive against the human protein. The following conjugated secondary antibodies were used (all 1:1000, ThermoFisher Scientific, validation provided on manufacturer's website): anti-Mouse IgG Alexa Fluor 488 (A21202), anti-Rabbit IgG Alexa Fluor 568 (A10042), and anti-Goat IgG Alexa Fluor 647 (A21447).

Eukaryotic cell lines

Policy information about cell lines

Cell line source(s)

Human fibroblasts were derived from patient skin-punch-biopsy samples, as described in Methods. iPSC lines were derived from these fibroblasts. CRISPR-edited hESC, and parent strain H9 hESC, which served as unedited controls, were obtained from WiCell.

Authentication

Fibroblast lines were morphologically confirmed as fibroblasts, and confirmed by sequence analysis to be both human and reference sequence at VCL and TPM variant loci. hESC and hiPSC lines were confirmed to be human by sequence analysis of the VCL and TPM1 loci, and positive for expression of pluripotency markers by immunofluorescence.

Mycoplasma contamination

Human fibroblast, human embryonic stem cell, and human induced pluripotent stem cell lines were tested regularly (Supplementary Table 7) for mycoplasma contamination by PCR analysis, and remained negative throughout the course of these experiments.

Commonly misidentified lines
(See ICLAC register)

No cell lines used in this study (H9 hESC, and patient-derived hiPSC and fibroblasts) are listed in the ICLAC database.

Animals and other organisms

Policy information about studies involving animals; ARRIVE guidelines recommended for reporting animal research

Laboratory animals

This information is reported in the "Mouse CRISPR-mediated genomic editing, genotyping, and colony maintenance" section in Methods. Briefly, all mice used were from the C57BL/6NHsd strain (Harlan Sprague Dawley Inc.) Mice were outcrossed to WT C57BL/6 mice for at least six generations, and were genotyped by either Sanger sequencing of target loci or by allele-specific PCR. All analyzed mice were male and between 15–59 weeks of age.

Wild animals

The study did not involve wild animals.

Field-collected samples

The study did not involve samples collected from the field.

Ethics oversight

All animal procedures were performed in accordance with National Institutes of Health guidelines and were approved by the UCSD Institutional Animal Care and Use Committee (Protocols #S13138 and S00138). UCSD has an Animal Welfare Assurance (#A3033-01) on file with the Office of Laboratory Animal Welfare and is fully accredited by AAALAC International.

Note that full information on the approval of the study protocol must also be provided in the manuscript.

Flow Cytometry

Plots

Confirm that:

☒ The axis labels state the marker and fluorochrome used (e.g. CD4-FITC).

☒ The axis scales are clearly visible. Include numbers along axes only for bottom left plot of group (a 'group' is an analysis of identical markers).

☒ All plots are contour plots with outliers or pseudocolor plots.

☒ A numerical value for number of cells or percentage (with statistics) is provided.

Methodology

Sample preparation	Individual hiPSC and hESC derived cardiomycytes were measured after trypsinization from their differentiation culture as described in the “Differentiation of human pluripotent stem cells (hPSCs) into cardiomyocytes” section in Methods.
Instrument	A BD LSRFortessa was used for data collection.
Software	BD FACSDiva software was used to collect data, and FlowJo v10 was used to analyze flow-cytometry data.
Cell population abundance	Positive expression of markers was assessed versus unstained controls.
Gating strategy	Standard FSC/SSC gating parameters were used to select single cells for analysis. Positive/negative staining boundaries were defined as the minimum fluorophore values for which >99.9% of negative control cells were negative.

☒ Tick this box to confirm that a figure exemplifying the gating strategy is provided in the Supplementary Information.